Broadband frequency and angular response of a sinusoidal Bull's-Eye antenna

U. Beaskoetxea[1], M. Navarro-Cía[2] and M. Beruete[1]

[1] *Antennas Group-TERALAB, Universidad Pública de Navarra, Campus Arrosadía, 31006 Pamplona, Spain*

[2] *School of Physics and Astronomy, University of Birmingham, Birmingham B15 2TT, UK*

E-mail: unai.beaskoetxea@unavarra.es, M.Navarro-Cia@bham.ac.uk and miguel.beruete@unavarra.es

A thorough experimental study of the frequency and beaming angle response of a metallic leaky wave Bull's-Eye antenna working at 77 GHz with a sinusoidally corrugated profile is presented. The beam scanning property of these antennas as frequency is varied is experimentally demonstrated and corroborated through theoretical and numerical results. From the experimental results the dispersion diagram of the $n = -1$ and $n = -2$ space harmonics is extracted, and the operation at different frequency regimes is identified and discussed. In order to show the contribution of each half of the antenna, numerical examples of the near-field behavior are also displayed. Overall, experimental results are in good qualitative and quantitative agreement with theoretical and numerical calculations. Finally, an analysis of the beamwidth as a function of frequency is performed, showing that it can achieve values below 1.5 deg in a fractional bandwidth of 4% around the operation frequency, which is an interesting frequency-stable broadside radiation.

I. INTRODUCTION

More than a decade ago, Extraordinary Transmission through a small aperture pierced on a periodically corrugated metallic plane was demonstrated, first at optical wavelengths [1] and then in other regimes of the electromagnetic spectrum such as microwaves [2] and millimeter-waves [3]. The corrugations have typically straight [4] or annular [5] shape and in the latter case, the structure is usually called Bull's-Eye (BE). An initial broadband analysis of the radiation mechanism was carried out in the optical regime for a BE structure in [6], where the correspondence between the field enhancement due to the presence of a groove array and the increase of transmission was studied. This work was complemented with the experimental analysis presented in [7] where the radiation of a BE was recorded and discussed for different setup combinations (number and periodicity of grooves, wavelength and angle of observation, parallel and perpendicular polarizations, etc.).

An interesting outcome for this type of structures is the possibility to obtain low-profile and all-metallic high-gain antennas, first reported at microwave frequencies [4,5,8], but nowadays extended to other frequencies such as millimeter-waves [9], terahertz (THz) [10] and even near-infrared band [11]. These antennas can be encompassed as a subclass of the leaky-wave antennas family [12–14] with the particularity that they can overcome their open stop-band limitation enabling high-gain broadside radiation. A remarkable application envisioned for these antennas is the shaping of the output beam of THz quantum cascade lasers [15]. Also, the relatively high-directivity along with the low-profile compared to horn or reflector antennas make

them interesting solutions for microwave as well as millimeter-wave applications, for instance in the automotive and aerospace sector [16].

Here we perform a broadband frequency analysis as well as a broad angular response characterization to understand better the operation of a BE antenna with a sinusoidal corrugation shape at a frequency range, millimeter-waves, where plasmonic models cannot be used. This way we intend to offer a thorough insight into the radiation mechanism of a BE with the idea of complementing the existing vast leaky-wave literature.

II. NUMERICAL, ANALYTICAL AND EXPERIMENTAL ANALYSIS

A description of the antenna can be found in our previous work [9] and is reproduced here in figure 1 (a-c) for the sake of completeness.

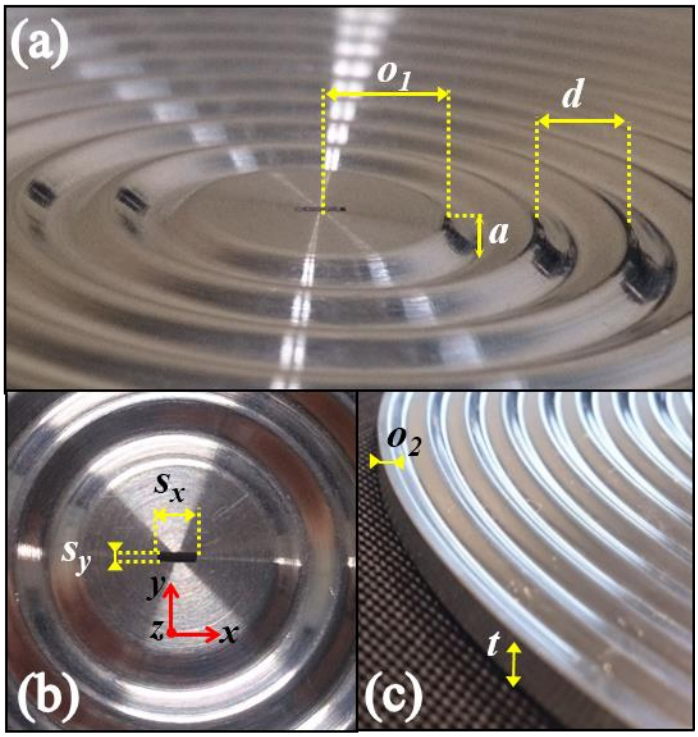

Figure 1. Fabricated prototype showing antenna's offset, o_1 = 5.1 mm, sine amplitude, a = 0.8 mm, and corrugation period, d = 3.89 mm (a); slot of dimensions $s_x \times s_y$ = 2.2 × 0.6 mm (b); and antenna thickness, t = 3.44 mm, and edge offset, o_2 = 0.8 mm, (c).

The simulated and experimental gain of the antenna as a function of frequency and angle were obtained at both principal planes, i.e. E-plane and H-plane [17], as described in the supplementary material [18]. The results of the experimental measurements are shown in figure 2 (a,c), for the E- and H-plane, respectively, and show good agreement with simulation results, figure 2 (b,d). From these results, the radiation and leaky wave parameters can be easily deduced showing clearly the radiation mechanism.

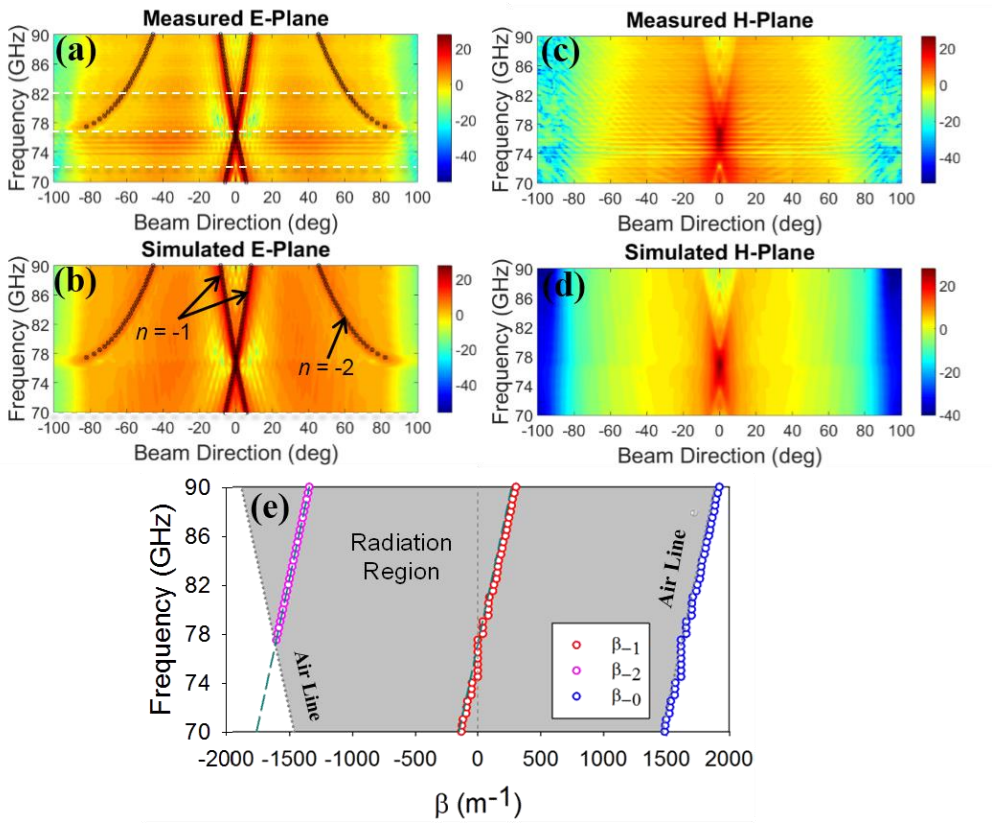

Figure 2. Experimental gain in dB for E-plane (a) and H-plane (c) as a function of angle and frequency. Simulated realized gain in dB for E-plane (b) and H-plane (d) as a function of angle and frequency. Dispersion diagram for modes n = 0 (blue circles), n = -1 (red circles) and n = -2 (pink circles) extracted from the measured beaming direction (e). Gray area indicates the fast wave or radiation region. Green dashed lines correspond to the analytically calculated phase constants.

As discussed in [12], leaky wave antennas present a scan-angle behavior, i.e. the beam direction can be changed with frequency. This is due to the fact that the phase constant β_n varies with frequency. In general, as frequency is swept the beam direction, θ_n, follows the next equation [13]:

$$\sin(\theta_n) = \frac{\beta_n}{k} = \frac{\beta_0}{k} + \frac{2\pi n}{kd} \tag{1}$$

where n is the index of the radiated space harmonic, β_n is the phase constant of the n-th space harmonic, β_0 is the phase constant of the n = 0 space harmonic (which corresponds to the travelling wave supported by a non-corrugated flat metallic plane, valid only for cases where the modulation is weak), $k = 2\pi/\lambda$ the free-space wavenumber and d the period of the periodic structure. In this structure, the wave propagates along a metal-air interface where the metal is a good electric conductor. Therefore, we can approximate $\beta_0 \approx k$. Based on this, we obtain:

$$\sin(\theta_n) \approx 1 + \frac{\lambda n}{d} \tag{2}$$

Thus, by means of (2), it is possible to estimate the beaming angle on the E-plane for each frequency given a certain periodicity. The calculated curves have been represented in figure 2 (a,b) overlapped to the measured and simulated results. As shown, they present a good matching with the beaming direction of the first pair of radiated space harmonics $n = -1$ and $n = -2$.

With the central slot excitation used, and due to the symmetry of the problem, currents are mainly directed along the *y*-*z* plane (E-plane, [17]), as shown in previous works [4,5]. The symmetry of the problem also imposes that the surface current along x is negligible. Consequently, the analytical description based on one-dimensional leaky-waves is meaningful only on the *y*-*z* plane. Hence, analytical lines are not overlaid in the *x*-*z* plane.

From (1) and extracting the beaming angle either from the experimental or numerical results of figure 2 (a,b), it is straightforward to deduce the phase constant of the leaky modes:

$$\beta_n = k\sin(\theta_n) \tag{3}$$

By applying this equation, the dispersion diagram of the $n = -1$ and $n = -2$ space harmonics are easily obtained, as depicted in figure 2(e). The phase constants calculated analytically, dashed green lines, are in good agreement with the curves obtained experimentally for both $n = -1$ and $n = -2$ modes. The phase constant for $n = 0$ (which is a bound mode and therefore inaccessible) was calculated by simply adding the term $2\pi/d$ to the phase constant of the $n = -1$ space harmonic. As shown in the figure 2(e), the $n = 0$ fundamental mode is always close to, but out of the radiation cone, as corresponds to a non-radiating mode [14]. Conversely, the $n = -1$ space harmonic is within the radiation cone for all the frequencies considered. From figure 2, three operation regimes can be distinguished:

(i) If $f < 77$ GHz then $\beta_{-1} < 0$, i.e. the leaky mode corresponds to a backward-wave. What is more, given the symmetry of the antenna, the upper and lower halves of the structure (defined with respect to the x-z plane located in the middle of the antenna and crossing along the slot length) radiate in opposite directions. This is clearly seen in figure 2(a, b) where two beams, corresponding to the $n = -1$ mode, are radiated in the range between 70 and 77 GHz in opposite directions. The beaming angle decreases with frequency, as corresponds to a backward-wave.

(ii) If $f \sim 77$ GHz then $\beta_{-1} \sim 0$, i.e. the leaky mode radiates at nearly broadside (direction of maximum radiation perpendicular to the plane of the antenna [19], which in this particular instance is $\theta = 0$deg.). This is also seen in figure 2 (a,b).

As frequency is swept towards the operation frequency f = 77 GHz, where $\lambda_0 \approx d$, the beams corresponding to each half of the antenna get gradually closer, pointing near θ = 0 deg and merging eventually into an apparently single broadside beam. It is noticeable the broadside beaming capability over a ~3.5 GHz bandwidth. As discussed in [20] pointing exactly at broadside is not possible, since this implies that β_{-1} must be exactly equal to zero. This is a singularity where the leaky mode becomes a standing wave, resulting in an open stop band in which radiated power sharply drops [13], [20].

(iii) Finally, if f > 77 GHz then $\beta_{-1} > 0$, i.e. the leaky mode corresponds to a forward-wave. Additionally, at f = 77 GHz a second pair of beams emerge near 90 deg. These beams correspond to the n = –2 space harmonic and within the frequencies considered is a backward-wave. So, in figure 2(a,b) four beams are identified. The ones closer to broadside are due to the n = –1 harmonic. The beaming angle increases with frequency, demonstrating that they correspond to a forward-wave. Conversely, the beams near endfire (direction along the plane of the antenna) are due to the n = –2 harmonic. In this case, the beaming angle decreases with frequency, demonstrating that they correspond to a backward-wave. The amplitude of the beams associated to the n = –2 space harmonic is comparatively inferior since the antenna was optimized for operation at the n = –1 space harmonic.

To illustrate the operation at each region, the E-plane radiation patterns at three different frequencies [corresponding to the dashed white lines of figure 2(a)] are plotted in figure 3. At f = 72 GHz two beams pointing at θ = ±3.3 deg are present (blue curve). This beams are due to the n = –1 space harmonic. Due to the inherent symmetry of the structure, both have the same gain amplitude of 18.1 dB. At f = 77 GHz, green curve, a single beam with a very high amplitude of 28.5 dB points in the broadside direction, whereas two low emerging lobes with amplitude 5.7 dB point near endfire, at θ = ±84 deg . These lobes correspond to the n = –2 mode [pink curve in figure 2(e)], which has entered the radiation cone, i.e. $|\beta_{-2}| < k_0$ so that this space harmonic is a fast wave. At f = 82 GHz, brown curve, in addition to the n = –1 beams pointing at θ = ± 4.4 deg, the n = –2 beams clearly appear pointing near θ = ±60 deg. In this case, the amplitude of the n = –1 beams decreases down to 16.5 dB, while n = –2 beams rise up to 5.9 dB. It can be seen that for the optimized f = 77 GHz case the sidelobe level (–23.9 dB) [21] is much lower than that of the other cases, (–15 dB and –12 dB at f = 72 GHz and f = 82 GHz, respectively).

In order to clarify further the beam scanning behavior of the antenna, we performed a simulation study using a two-dimensional (2D) equivalent structure similar to that presented in [22]. Details of the simulation can be found in the supplementary material. The H_x field distribution of the n = –1 mode at f = 60 GHz, f = 77 GHz, f = 82 GHz and f = 90 GHz on the E-plane is shown in figure 4. The H_x component is chosen for the analysis because, due to the symmetry of the problem, the wave radiated by the central slot is a TM_z mode.

When the frequency is below f = 77 GHz, $\lambda > d$, each half of the structure radiates in the opposite half-plane. Figure 4(a) shows that at f = 60 GHz the upper-half of the antenna radiates in the lower-half plane direction and the lower-half vice versa. Both beams create a central zone near the surface of the structure with strong field concentration. As frequency is swept towards f = 77 GHz, both beams get closer, merging at f = 77 GHz into an apparently single beam pointing at θ = 0 deg, due to the parallel beam radiation of both upper and lower halves, figure 4(b). Above f, the single broadside beam splits again in two. Figures 4(c) and (d) display the performance at f = 82 GHz and f = 90 GHz, respectively. For $\lambda < d$, each half of the antenna radiates in its own half-plane and both beams get further apart as the frequency is increased.

A parameter of paramount importance in antennas is the half-power beamwidth (θ_{-3dB}). Figure 5 shows the θ_{-3dB} beamwidth as a function of frequency for experimentally and numerically analyzed 20 period BE antenna along with the experimental E-plane radiation diagrams at each tagged frequency (b-e).

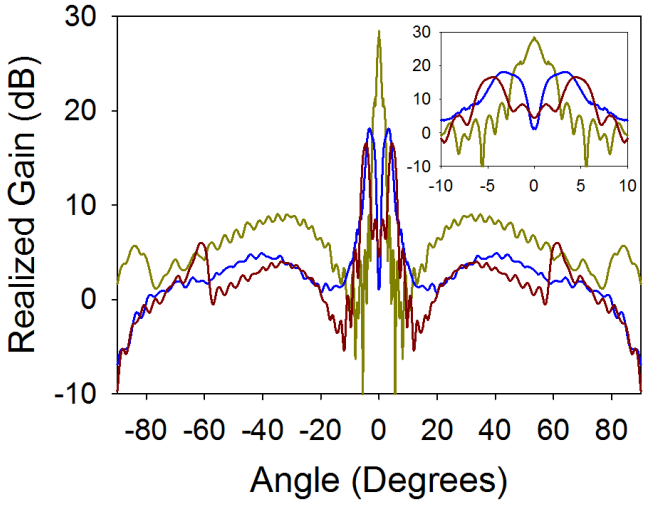

Figure 3. Experimental E-plane radiation pattern at f = 72 GHz (blue curve), f = 77 GHz (green curve) and f = 82 GHz (brown curve). Inset: Detail of the beam splitting.

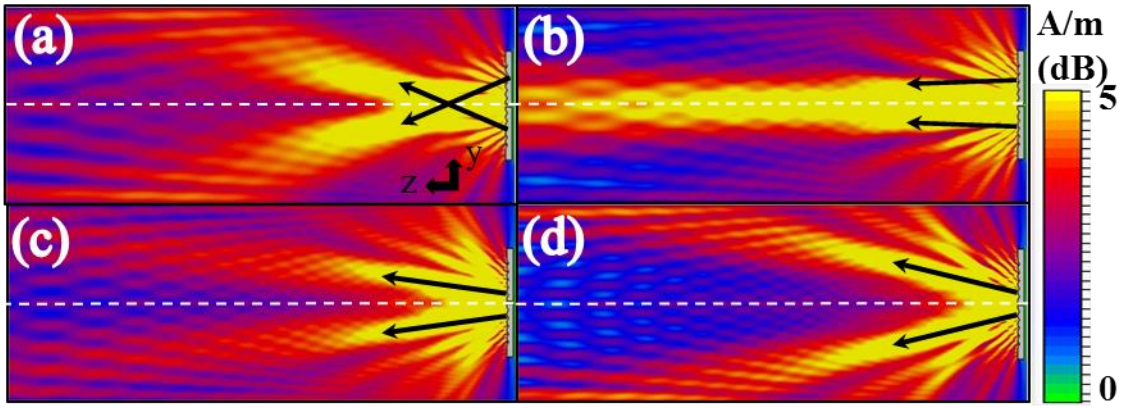

Figure 4. Contour plot of the simulated magnitude of H_x at the E- cutting plane at f = 60 GHz (a), f = 77 GHz (b), f = 82 GHz (c) and f = 90 GHz (d).

The largest beamwidth values are found at f = 73.5 GHz (b) and f = 77.6 GHz (d), where θ_{-3dB} = 5.6 deg and θ_{-3dB} = 4.4 deg respectively. At these frequencies, the beams corresponding to each half are so near that they cannot be resolved separately, appearing as a wider single beam, with large θ_{-3dB} value. At the design frequency, f = 77 GHz, a narrow θ_{-3dB} = 1.2 deg pencil shape beam is observed, whereas for frequencies above f = 79 GHz, beams are slightly wider. At f = 82 GHz (e), for example, a θ_{-3dB} = 2 deg beam is recorded. It can be observed that the mean beamwidth value follows a decreasing tendency, due to the well-known directivity enhancement as the wavelength gets shorter. Meanwhile, the observed red-shifting of the experimental results with respect to the simulation results can arguably be assigned to fabrication tolerances, given the known high sensitivity of the operating frequency to the corrugation period. Narrower bandwidths recorded at higher frequencies (77 – 79 GHz) might be due to fabrication tolerances as well as to the fact that simulations show far-field results, whereas our measurements, due to experimental set-up space constraints, are not rightly far-field (and no near-field to far-field transformation has been applied). It is interesting to observe that within the range of f = 74.2 GHz to f = 77.3 GHz (4% fractional bandwidth), the measured θ_{-3dB} values are below 1.5 deg. This is certainly a positive feature which demonstrates that the antenna beamwidth is stable around the design frequency.

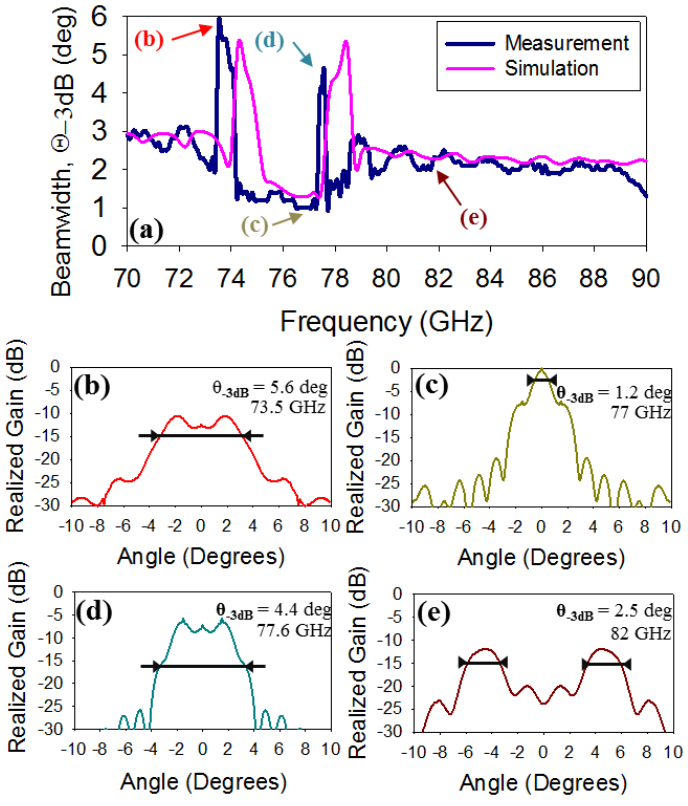

Figure 5. Experimental (blue curve) and simulated (pink curve) beamwidth as a function of frequency (a). E-plane radiation pattern near broadside for f = 74.25 GHz (b), f = 77 GHz (c), f = 78.5 GHz (d) and f = 82 GHz (e). Black arrows mark the θ_{-3dB} interval.

III. CONCLUSION

To conclude, in this work a thorough review of the beam scanning behavior of a metallic BE antenna with sinusoidal profile working at 77GHz is presented. It has been experimentally proven the variation of the beaming angle as the operating frequency is swept, observing a good agreement between numerical, measured and theoretically predicted values. The phase constant has been obtained from measurements for $n = 0, -1$ and -2 Floquet modes. By means of the dispersion diagram, a qualitative analysis of the different radiation regions has been done. It has been experimentally demonstrated that the high gain at broadside is due to the merging of the beams radiated by each half of the antenna. This explanation has been reinforced by means of a graphical analysis of the H_x field distribution at different frequencies. The beamwidth vs frequency has been obtained showing that it is minimum at the design frequency but it is flanked by two regions where it increases abruptly due to the merging of the beams radiated by each part of the antenna, appearing as a wider single beam. Relatively narrow beamwidths below 1.5 deg within an interval near the design frequency f = 77GHz (from 74.2 GHz to 77.3 GHz) are obtained with pencil beam shape. In this bandwidth an interesting frequency-stable broadside radiation is also observed. It is shown that the beamwidth remains small and constant as the beam is frequency scanned around the design frequency. The results shown in this work are of interest for novel designs involving this type of antennas, especially at THz frequencies.

ACKNOWLEDGMENTS

This work was supported by the Spanish Government under contract TEC2014-51902-C2-2-R. M. N.-C. is supported by University of Birmingham [Birmingham Fellowship]. M.B. acknowledges support by the Spanish Government under contract RYC-2011-08221

REFERENCES

[1] Lezec H J, Degiron A, Devaux E, Linke R A, Martin-Moreno L, Garcia-Vidal F J and Ebbesen T W 2002 Beaming light from a subwavelength aperture *Science.* **297** 820–2

[2] Beruete M, Campillo I, Dolado J S, Rodríguez-Seco J E, Perea E and Sorolla M 2004 Enhanced microwave transmission and beaming using a subwavelength slot in corrugated plate *IEEE Antennas Wirel. Propag. Lett.* **3** 328–31

[3] Navarro-Cía M, Beruete M, Campillo I and Sorolla M 2009 Millimeter-Wave Left-Handed Extraordinary Transmission Metamaterial Demultiplexer *IEEE Antennas Wirel. Propag. Lett.* **8** 212–5

[4] Beruete M, Campillo I, Dolado J S, Perea E, Falcone F and Sorolla M 2006 Dual-band low-profile corrugated feeder antenna *IEEE Trans. Antennas Propag.* **54** 340–50

[5] Beruete M, Campillo I, Dolado J S, Rodríguez-Seco J E, Perea E, Falcone F and Sorolla M 2005 Very Low-Profile "Bull's Eye" Feeder Antenna *IEEE Antennas Wirel. Propag. Lett.* **4** 365–8

[6] Carretero-Palacios S, Mahboub O, Garcia-Vidal F J, Martin-Moreno L, Rodrigo S G, Genet C and Ebbesen T W 2011 Mechanisms for extraordinary optical transmission through bull's eye structures. *Opt. Express* **19** 10429–42

[7] Yi J-M, Cuche A, Devaux E, Genet C and Ebbesen T W 2014 Beaming Visible Light with a Plasmonic Aperture Antenna *Acs Photonics* **1** 365–70

[8] Beruete M, Campillo I, Dolado J S, Rodríguez-Seco J E, Perea E, Falcone F and Sorolla M 2005 Low-Profile Corrugated Feeder Antenna *IEEE Antennas Wirel. Propag. Lett.* **4** 378–80

[9] Beaskoetxea U, Pacheco-Peña V, Orazbayev B, Akalin T, Maci S, Navarro-Cía M and Beruete M 2015 77 GHz High Gain Bull's-Eye Antenna With Sinusoidal Profile *IEEE Antennas Wirel. Propag. Lett.* **14** 205–8

[10] Beruete M, Beaskoetxea U, Zehar M, Agrawal A, Liu S, Blary K, Chahadih A, Han X L, Navarro-Cia M, Etayo Salinas D, Nahata A, Akalin T and Sorolla M 2013 Terahertz Corrugated and Bull ' s-Eye Antennas *IEEE Trans. Terahertz Sci. Technol.* **3** 740–7

[11] Ren F F, Ang K W, Ye J, Yu M, Lo G Q and Kwong D L 2011 Split bull's eye shaped aluminum antenna for plasmon-enhanced nanometer scale germanium photodetector *Nano Lett.* **11** 1289–93

[12] Monticone F and Alù A 2015 Leaky-Wave Theory, Techniques, and Applications: From Microwaves to Visible Frequencies *Proc. IEEE* **103** 793–821

[13] Oliner A A and Jackson D R 2007 Leaky-Wave Antennas *Antenna Engineering Handbook* ed J L Volakis (New York: Mc Graw-Hill) pp 11–1/11–56

[14] Baccarelli P, Burghignoli P, Lovat G and Paulotto S 2004 A novel printed leaky-wave "bull-eye" antenna with suppressed surface-wave excitation *IEEE Antennas and Propagation Society Symposium, 2004.* vol 1 (IEEE) pp 1078–81 Vol.1

[15] Yu N, Fan J, Wang Q J, Pflügl C, Diehl L, Edamura T, Yamanishi M, Kan H and Capasso F 2008 Small-divergence semiconductor lasers by plasmonic collimation *Nat. Photonics* **2** 564–70

[16] Vourch C J and Drysdale T D 2014 V-band "bull"s eye' antenna for cubeSat applications *IEEE Antennas Wirel. Propag. Lett.* **13** 1092–5

[17] In antennas with linear polarization the E-plane is defined as the cutting-plane that contains the electric field vector

and the direction of maximum radiation. For the antenna considered here, it coincides with the *y*-*z* middle-plane. Likewise, the H-plane is defined as the cutting-plane that contains the magnetic field vector and the direction of maximum radiation. In the manuscript we identify the H-plane with the *x*-*z* middle-plane, although strictly speaking they only coincide at the design frequency where broadside radiation occurs.

[18] See supplementary material at {DOI} for description of the antenna, experimental setup and measurement details and numerical modelling details.

[19] IEEE Antennas and Propagation Society 1993 *IEEE Standard Definitions of Terms for Antennas* vol 2013

[20] Jackson D R, Oliner A A, Zhao T and Williams J T 2005 Beaming of light at broadside through a subwavelength hole: Leaky wave model and open stopband effect *Radio Sci.* **40** 1–12

[21] The sidelobe level is defined as the ratio between the highest secondary lobe and the maximum of the main lobe, expressed in dB.

[22] Martín-Moreno L, García-Vidal F J, Lezec H J, Degiron A and Ebbesen T W 2003 Theory of highly directional emission from a single subwavelength aperture surrounded by surface corrugations *Phys. Rev. Lett.* **90** 167401